nature mental health

Article

https://doi.org/10.1038/s44220-024-00275-5

Tumor location is associated with mood dysfunction in patients with diffuse glioma

Received: 3 August 2023

Accepted: 29 May 2024

Published online: 11 July 2024

Check for updates

Maisa N. G. van Genderen[1,2,9], Vera Belgers[2,3,9], Johanna M. Niers[2,3], Linda Douw[2,4,5], Jantine G. Röttgering[2,6], Maxine Gorter[2,4], Marieke E. C. Blom[2,4], Frederik Barkhof[5,7,8], Martin Klein[2,6], Roelant S. Eijgelaar[1,2] & Philip C. De Witt Hamer[1,2]

Gliomas are primary brain tumors that can cause neuropsychiatric symptoms, including severe depressive symptoms (SDS; in 14%) and an absence of depressive symptoms (ADS; in 29%), determined by Center for Epidemiologic Studies Depression (CES-D) scores. We examined the association between both SDS and ADS and brain tumor location in 201 patients with diffuse glioma before surgery. Tumors and white matter disconnectomes did not relate to CES-D using sparse canonical correlation analysis. SDS were associated with tumors in the right corticospinal tract, fornix, and inferior fronto-occipital fasciculus and the left uncinate fasciculus, whereas ADS was associated with tumors in the left uncinate fasciculus and first segment of the superior longitudinal fasciculus and the right temporal cingulum and thalamus using Bayesian regression analyses. ADS occurs even more frequently in patients with diffuse glioma than does SDS, which is explained partly by tumor location. This research aids the understanding of gliomas and mood dysfunction in general.

Diffuse gliomas are the most common and most deadly primary malignant brain tumors[1,2]. They are characterized by infiltrative growth and can cause a wide range of neurological, cognitive, and neuropsychiatric symptoms[3,4]. Patients with diffuse glioma commonly undergo surgical resection as a first treatment step[4].

After any cancer diagnosis, patients often experience sadness and distress during a few weeks to months, and depressive symptoms usually peak shortly after cancer diagnosis[5,6]. While it is understandable that patients recently diagnosed with life-threatening diseases may exhibit certain depressive symptoms, severe depressive symptoms are burdensome and negatively affect quality of life[7]. Up to 54% of preoperative patients with brain tumors report depressive symptoms, which is more frequent than in other cancer types and may be explained by patient characteristics, psychometric properties of the questionnaires used, or possibly the tumor location[8,9].

As some depressive symptoms are congruent with recent bad news of the incurable nature of the disease and information on treatment-related risks, an absence of depressive symptoms seems discrepant. An absence of depressive symptoms has not been reported on before but could possibly reflect a maladaptive response such as emotional blunting. Emotional blunting, the numbing of both positive and negative feelings, has been described in brain tumor patients, as has apathy[10–12]. Emotional blunting is related to impaired functioning and reduced quality of life[13]. We hypothesize that the presence of intracranial lesions that disturb brain functions could contribute to severe depressive symptoms and an absence thereof[10,11].

For many brain diseases, including glioma, symptoms have been mapped to lesion locations to find relations between symptoms and brain structures[14–16]. This mapping is traditionally analyzed by

[1]Amsterdam UMC location Vrije Universiteit Amsterdam, Neurosurgery, Amsterdam, the Netherlands. [2]Cancer Center Amsterdam, Brain Tumor Center, Amsterdam, the Netherlands. [3]Amsterdam UMC location Vrije Universiteit Amsterdam, Neurology, Amsterdam, the Netherlands. [4]Amsterdam UMC location Vrije Universiteit Amsterdam, Anatomy and Neurosciences, Amsterdam, the Netherlands. [5]Amsterdam UMC, Amsterdam Neurosience, Vrije Universiteit, Amsterdam, the Netherlands. [6]Amsterdam UMC location Vrije Universiteit Amsterdam, Medical Psychology, Amsterdam, the Netherlands. [7]Amsterdam UMC location Vrije Universiteit Amsterdam, Radiology and Nuclear Medicine, Amsterdam, the Netherlands. [8]Queen Square Institute of Neurology and Centre for Medical Image Computing, University College London, London, UK. [9]These authors contributed equally: Maisa N. G. van Genderen, Vera Belgers. e-mail: p.dewitthamer@amsterdamumc.nl

https://doi.org/10.1038/s44220-024-00275-5

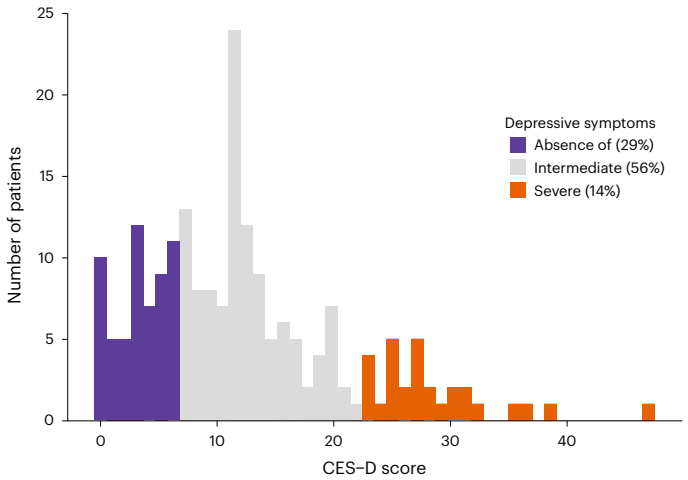

Fig. 1 | Distribution of depressive symptom scores and corresponding categories. Number of patients versus CES-D score.

voxel-based lesion symptom mapping, which suffers from poor correction of multiple testing and ignores spatial correlations between voxels[17]. Therefore, spatial brain relations are preferably taken into account as these are more likely to explain symptoms[18–20]. Mapping symptoms to brain regions as a whole and brain networks of connected regions can be a rich source of information that can be applied to routine clinical imaging[21–23].

In stroke, depressive symptoms are related to the location of the lesion, such as the prefrontal cortex and the thalamocortical and dorsal frontal white matter tracts[24–26]. However, differences in pathophysiological mechanisms between stroke and diffuse glioma may result in distinct lesion symptom associations[27]. Few studies investigated the association between brain tumor location and depressive symptoms; none investigated the absence thereof. Previous studies found no association between depressive symptoms and lobar involvement but lacked more detailed brain parcellations[8,28,29]. One study summarized 18 published case reports of patients with depression and found 89% of the depression-related tumors were functionally connected to the left striatum, the putamen, and the pallidum, according to voxel-wise analysis[30].

In this study, we hypothesize that tumor location is related to both severe depressive symptoms and an absence of depressive symptoms in preoperative patients with diffuse glioma. To gain insight into the neuroanatomy and etiology of these phenomena, we mapped depression scores to brain regions and networks with tumor infiltration and their corresponding disconnected regions. We applied several methods: (1) a data-driven cluster analysis without pre-defined regions, (2) a lesion load analysis including white matter and cortical and subcortical gray matter parcels, (3) probability of involvement of white matter tracts, and (4) modeled functional network impact; see Extended Data Figs. 1 and 2 for an overview of methods.

Results

Patient population

We identified 203 patients with a newly diagnosed diffuse glioma who completed the Center for Epidemiologic Studies Depression scale (CES-D) within a year before surgery. Two patients were excluded from the analysis due to poor registration of their magnetic resonance imaging (MRI) to standard brain space, which resulted in 201 patients with characteristics as listed in Extended Data Tables 1–3.

Depressive symptom distribution and categories

An absence of depressive symptoms (CES-D ≤ 6) occurred in 29% of patients and severe depressive symptoms (CES-D ≥ 23) in 14% of patients (Fig. 1).

Clinical characteristics

Of the patient characteristics, female sex (mean regression coefficient (RCμ) = 1.10, 94% posterior highest density interval ($HDI_{94\%}$) = 0.18–2.03) was associated with severe depressive symptoms, and high Verhage educational level (RCμ = 0.95, $HDI_{94\%}$ = 0.15–1.81) and high 36-Item Short Form (SF-36) physical functioning score (RCμ = 0.09, $HDI_{94\%}$ = 0.05–0.14) were associated with an absence of depressive symptoms. None of the other patient or tumor characteristics was significantly associated with either CES-D category.

Tumor and disconnectome distributions

The maps of the segmented tumor locations are shown in Fig. 2a, for both the complete group and split by depressive symptom category. We also created disconnectomes based on normative tractography, which reflect white matter tracts that are likely affected by a tumor lesion, as shown in Fig. 2b. When tested using sparse canonical correlation analysis (Extended Data Fig. 1; cluster-based analyses), tumor and disconnectome locations were not significantly associated with CES-D.

Tumor and disconnectome load

We then tested tumor load and disconnectome load on pre-defined brain regions using Bayesian categorical regression (see Extended Data Fig. 2: Lesion load). The load was calculated by dividing the lesion volume within a region by the total region volume.

Tumor load in the right thalamus was significantly associated with an absence of depressive symptoms (RCμ = 7.60, $HDI_{94\%}$ = 1.19–14.43) (Fig. 3). See Fig. 5 and Supplementary Fig. 2 for all associations. Tumor load in the white matter tracts or cortical functional regions and disconnectome load on white matter tracts were not associated with CES-D category.

White matter tract involvement

Next, we tested whether the probability of involvement, also known as the probability of disconnection, related to depressive symptom categories (see Extended Data Fig. 2: Probability of involvement). Severe depressive symptoms were associated with white matter tract involvement of the right corticospinal tract (CST; RCμ = 4.63, $HDI_{94\%}$ = 1.02–8.43), the right fornix (RCμ = 11.31, $HDI_{94\%}$ = 6.62–15.50), the right inferior fronto-occipital fasciculus (IFOF; RCμ = 5.21, $HDI_{94\%}$ = 0.24–10.30), and the left uncinate fasciculus (RCμ = 6.30, $HDI_{94\%}$ = 2.08–10.12) (Fig. 4a).

Interestingly, involvement of the left uncinate fasciculus was also significantly associated with an absence of depressive symptoms (RCμ = 3.65, $HDI_{94\%}$ = 1.16–6.00) (Fig. 4b). In addition, involvement of the right temporal cingulum (RCμ = 5.88, $HDI_{94\%}$ = 1.96–9.61) and the left superior longitudinal fasciculus (RCμ = 1.98, $HDI_{94\%}$ = 0.33–3.81) were significantly associated with an absence of depressive symptoms. See Fig. 5 and Supplementary Fig. 2 for all correlations.

Modeled functional network impact

Last, we modeled the potential impact of the tumor on functional networks using large normative functional network data. We calculated impact on graph measures local efficiency and eigenvector centrality to evaluate its relation to depressive symptom categories (Extended Data Fig. 2: Functional network impact). We found no significant associations.

Discussion

We explored how severe depressive symptoms and an absence thereof related to tumor and disconnectome locations and modeled functional network impact in patients with supratentorial diffuse glioma. The locations of tumors, in addition to established patient-related risk factors, were related to these extremes of depression scores.

https://doi.org/10.1038/s44220-024-00275-5

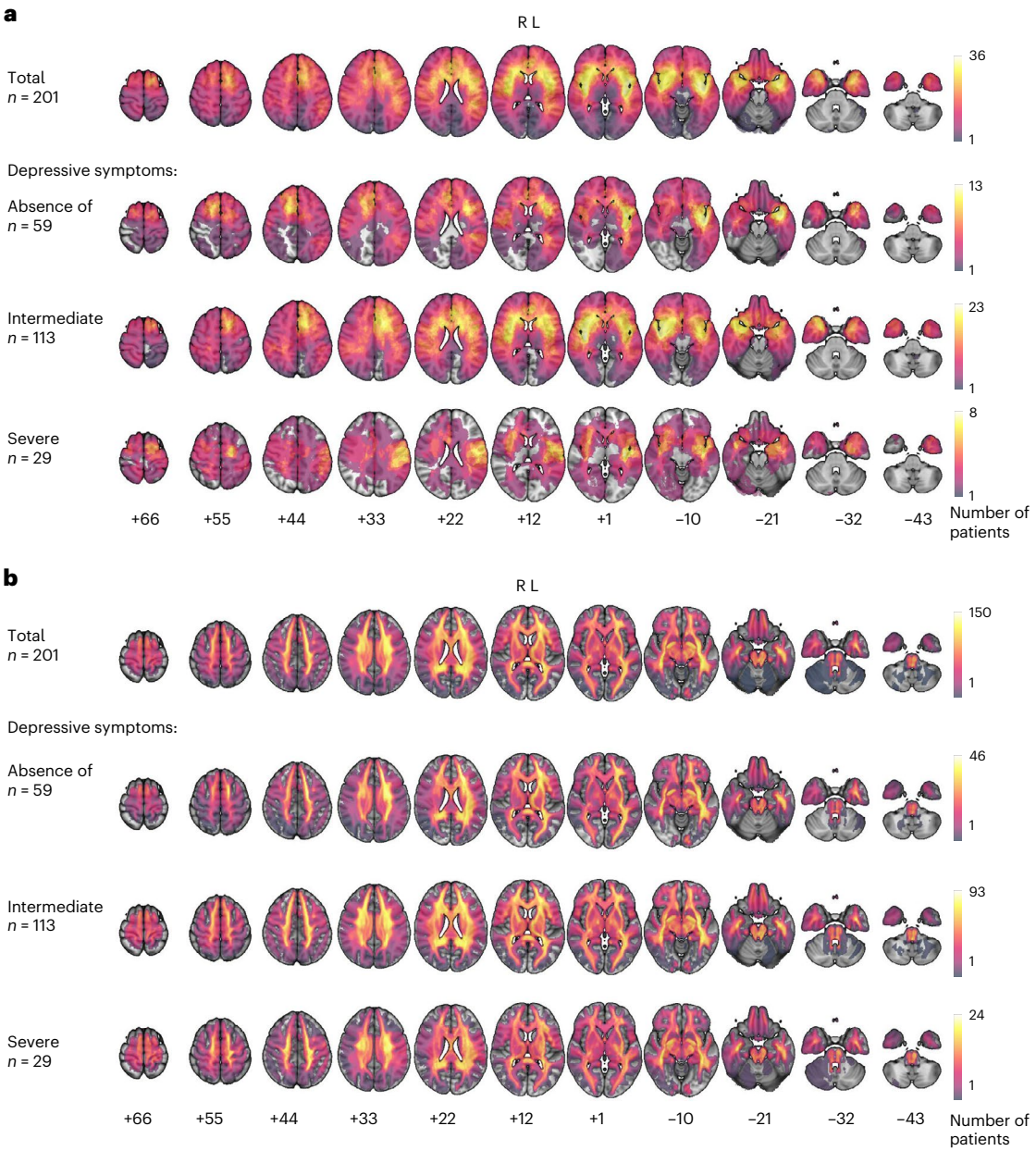

Fig. 2 | Distribution maps for the total population by depressive symptom categories. a, For tumor locations. **b**, For disconnectome locations. The color legends to the right indicate the number of patients with tumors overlapping at a voxel location; the maximum numbers vary by category. The plotted numbers below refer to Montreal Neurological Institute 152 standard space *z*-axis slice. L, left; R, right.

Our findings confirmed that severe depressive symptoms occurred in 14% of patients with brain tumors and that female sex is a risk factor[31]. In addition, we found structures of the limbic system to be related to severe depressive symptoms (the right fornix and the left uncinate fasciculus)[32] as well as regions involved in movement and in language, goal-oriented behavior, and visuospatial attention (the right CST and the right IFOF)[33].

These results are in line with findings in major depressive disorder, where the limbic–thalamo–cortical circuit is pivotal[34]. Specific depressive symptoms have been associated with specific regions and circuits[35], for example, the fornix in memory, disrupted cognitive control, and self-referential thought[32,36,37]. The uncinate fasciculus is involved in integrating visceral and emotional information, and dysfunction can result in cognitive and behavioral problems[32]. Furthermore, brain–depression relations have also been investigated in depression secondary to neurologic disorders. Post-stroke depression is most widely examined, and studies have found anterior structures, the reward circuit, and limbic structures to be involved[26,38]. Studies into depression after brain diseases other than stroke have identified similar regions, including the uncinate fasciculus, IFOF, CST, and frontolimbic circuits[39–41].

In addition to these limbic structures, the right IFOF was related to severe depressive symptoms and has been implicated in nonverbal semantic processing and visuospatial awareness[42,43]. Possibly, lesions in this region result in more disability and consequently depression[44]. Indeed, the IFOF has been related to post-stroke depression and major depressive disorder, possibly as a result of cognitive changes[45,46]. A similar secondary mechanism could drive involvement of the CST with voluntary movement. Perhaps lesions in these areas result in more physical disability, resulting in more depressive symptoms although we did consider functional impairment as a covariate[47].

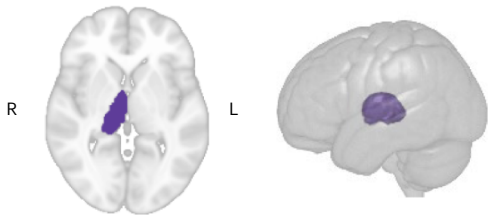

Fig. 3 | Tumor load significant associations with depressive symptom categories. The right thalamus is associated with an absence of depressive symptoms. Here visualized in two dimensions and three dimensions. L, left; R, right.

We identified an absence of depressive symptoms in 29% of patients, which we considered remarkably high. Higher educational level related to an absence of depressive symptoms, corroborating earlier research[31,48]. In addition, higher scores on physical functioning related to an absence of depressive symptoms. Taking educational level, sex, and physical functioning into account, regions involved in an absence of depressive symptoms included the limbic regions right temporal cingulum, right thalamus and left uncinate fasciculus, and left SLF 1.

An absence of depressive symptoms is likely to be multifactorial in origin. In general, after a cancer diagnosis, a delayed realization of illness can occur, possibly contributing to an absence of depressive symptoms in the first phase[49]. In addition, resilience and even thriving can develop after cancer diagnosis and can relate to an absence of depressive symptoms. However, this generally occurs later in the disease and would therefore not explain the high prevalence we observed[50]. In addition, denial of cancer diagnosis could contribute to an absence of depressive symptoms. In newly diagnosed lung cancer patients, high levels of denial occurred in 3% of patients and indeed related to fewer depressive symptoms[51,52]. Indeed, brain tumor patients have been described to underestimate their problems compared with their caregivers, which has been hypothesized to be due to reduced insight or denial[53]. Another neuropsychiatric explanation may be anosognosia: the absence of awareness of a disease or dysfunction. Anosognosia occurs in around 10% of acute stroke patients and is related to worse functional outcomes[54]. However, the literature remains inconclusive on whether anosognosia relates to more or fewer depressive symptoms[55–59]. An absence of depressive symptoms could also reflect dysfunction of the mood circuitry. Indeed, the fornix, which in our study was related to severe depressive symptoms, has previously been associated with apathy[60–62]. Moreover, we found the left uncinate fasciculus to be associated with both severe depressive symptoms and an absence of depressive symptoms, suggesting the potential for a dual response to its dysfunction.

Finally, an absence of depressive symptoms could indicate emotional blunting, which is an absence of emotional response to an emotional stimulus such as a cancer diagnosis, or apathy, defined as diminished goal-directed behavior and decreased emotion or feelings or interest[63,64]. Apathy does have characteristics in common with depression, such as no desire to pursue reward, but it is a unique entity with decreased emotion rather than feelings of depression[65,66]. Both emotional blunting and apathy are related to worse functional outcomes and reduced quality of life[13,67]. Emotional blunting and apathy have been reported after brain lesions and are common in neurodegenerative diseases. Regions associated with an absence of depressive symptoms in our cohort have previously been described in apathy and emotional blunting: the thalamus is involved in decreased emotional responses and cognitive processes[68], and lesions in this region are related to post-stroke apathy and worse self-reported cognitive functioning[69,70]. In neurodegenerative diseases, apathy has been associated with white matter alterations in limbic structures: the temporal cingulum and the uncinate fasciculus[62,71–73], which are involved in motivation[63]. In schizophrenia, negative symptoms have also been associated with alterations in the temporal cingulum[74,75]. This could be due to memory formation and retrieval[74] or due to absence of interest or emotional reactivity[62]. The superior longitudinal fasciculus has also been associated with apathy in various populations[62,71–73,76,77], the SLF 1 specifically with attention[78].

In summary, an absence of depressive symptoms could stem from various mechanisms. Considering the high prevalence of an absence of depressive symptoms in our glioma population, a neuropsychiatric basis such as a dysfunction of the mood circuitry or emotional blunting seems plausible. We encourage future research to explore this phenomenon and its etiologies.

Our findings confirm the importance of the limbic system both in depressive symptoms and in an absence of depressive symptoms. However, contrary to associations found in (post-stroke) depression and apathy, we found no evidence of neocortical regions interfering with the limbic system in glioma patients. Specifically, the dorsolateral prefrontal cortex, as part of the frontoparietal network, seems crucial in depression and apathy following stroke[26,68,79]. However, in our study, tumors in this region were not associated with depression scores. In general, depression could be the result of hypoactivity of the cortex or hyperactivity of the limbic system[80]. Brain tumors possibly increase the activity of the limbic system rather than decrease cortical regulation of the limbic system as brain tumors have been shown to increase neuronal activity[81]. This may explain why different brain lesion etiologies can cause different lesion symptom results:[27,30] in patients with gliomas, the brain is functionally disturbed at distance from the tumor[82–85]. The interaction between tumors and the surrounding brain seems to be bidirectional: not only does increased neuronal activity promote tumor growth[86,87], the tumor also induces both neuronal death and neuronal hyperexcitability and can increase and decrease peritumoral connectivity[88–92]. In support of this, glioblastomas have been demonstrated to modify neural circuits by overactivating brain areas around language regions found in healthy individuals[90]. We speculate that neural circuits involved in mood regulation, such as depressive symptoms, may also be remodeled by glioma by both hyperactivity and hypoactivity. Further research is required in this emerging field of cancer neuroscience.

In this Article, we adopted a rigorous design with several methods to investigate the association between depressive symptoms and tumor location. Not all methods identified a lesion–depression correlation. First, the cluster-based analysis yielded no regions associated with depression scores, possibly because the tumors are too large to identify small regions: LESYMAP has been developed in the context of stroke, in which the lesions are possibly smaller. Moreover, we used the continuous CES-D to relate to clusters, and a nonlinear relation between a brain region associated with both extremes of depression scores may not become apparent by assuming linearity. Furthermore, the statistical power to detect an association is not equally distributed over brain regions, varying by preferential locations of tumors, so that relevant brain regions may remain undetected. Second, the disconnectome of a tumor may incorrectly conceptualize an entire loss of function from disconnection. Similarly, the lesion load does not necessarily reflect a complete loss of function of the tumor-infiltrated brain region. In addition, especially in white matter tracts, a specific location within the tract may be more important than lesion load, for example, in a location with higher axonal density[93]. The dysfunction of a white matter tract is presumably better reflected by the probability of a tumor involving that tract, capturing switch-like functional intactness[94]. Third, modeled functional network impact also did not relate to depressive symptoms. Brain tumors presumably interfere more dynamically with the network than our modeled one-time differences, which is probably more fitting with stroke[27]. However, a better model of the effects of a growing tumor

https://doi.org/10.1038/s44220-024-00275-5

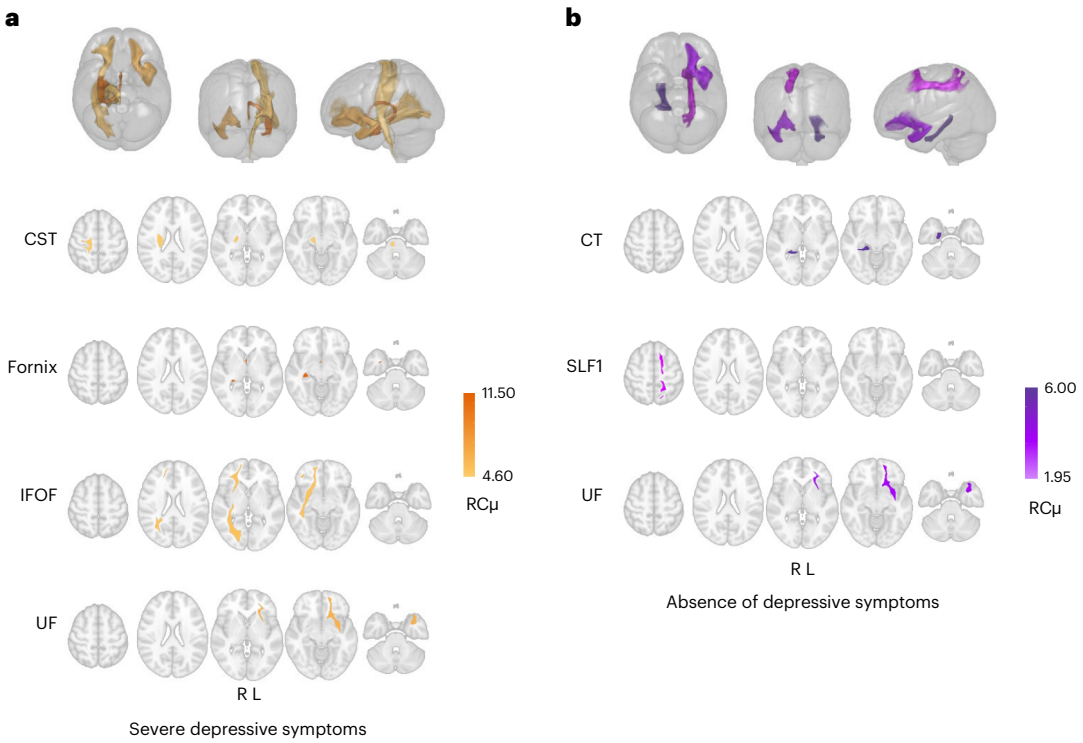

Fig. 4 | White matter tract involvement has significant associations with depressive symptom categories. a, White matter tracts where involvement was associated with severe depressive symptoms. From top to bottom: a 3D overview of all associated tracts, the right corticospinal tract (CST), the right fornix, the right fronto-occipital fasciculus (IFOF), and the left uncinate fasciculus (UF). **b**, White matter tracts where involvement was associated with an absence of depressive symptoms. From top to bottom: a 3D overview of all associated tracts, the right temporal cingulum (CT), the left first segment of the superior longitudinal fasciculus (SLF 1), and the left UF. The color intensities represent the RCμ. L, left; R, right.

on the functional network does currently not exist to our knowledge. Nevertheless, an alternative approach using voxel-wise or peak cluster analysis to lesion network mapping, as described in other work[21,24,79,95], may illuminate new associations between the functional network and depressive symptoms and could be considered in future work.

Limitations

Our study also highlights some challenges of tumor lesion symptom mapping. First, tumors do not have an acute onset with complete loss of function of normal brain tissue, but develop gradually over time and may result in partial loss of function given their infiltrative nature. This gradual growth often induces neuroplasticity, and therefore lesion symptom mapping in brain tumors and stroke could result in different findings[27,30,96,97]. Nevertheless, most of our findings corroborate the brain–depression literature. Second, tumor segmentation is subject to inter- and intra-rater variability, although this is usually not a major source of variation[98]. Third, tumor extent may be underestimated as there is diffuse involvement outside the focal lesion. Fourth, the unknown combination of expansive and infiltrative growth of the tumor makes registration to standard space inherently challenging[99]. To minimize these errors, all segmentations and registrations were visually verified in 3D Slicer. Fourth, the combined error from previous arguments may also lead to spatial bias and thus potential misinterpretation of tumor location in atlas space. In addition, the parcels of brain atlases do not necessarily represent units of depressive symptoms. Furthermore, we disregarded the anticorrelations as the interpretation of a brain region safeguarding against a dysfunction on tumor infiltration remains elusive[21,95]. In addition, we used the CES-D as a single measure of depressive symptoms within a month of a major surgical procedure. The CES-D focuses primarily on symptom frequency rather than intensity[100], and this may be temporarily elevated before surgery, in particular in patients with neurologic deficits. For a thorough diagnosis of mood (dys)function in the complex circumstances following a grave tumor diagnosis and facing a major surgical procedure, diagnostic interviews by psychiatric professionals would be required. Moreover, no consensus on a cut-off for an absence of depressive symptoms exists. We undertook our best efforts, using several methods, to establish a convincing cut-off, and our findings align with clinical observations of apathy at presentation in patients with newly diagnosed glioma[101]. Still, verifying this phenomenon by comparing CES-D with other populations who just received a grave diagnosis would be advisable. Last, our population may be subject to selection bias. Patients with insufficient capacity to fill out the CES-D questionnaire were unavoidably missing from this analysis, possibly underestimating mood dysfunction.

Conclusions

Patients with supratentorial diffuse glioma experience both severe depressive symptoms (14%) and an absence of depressive symptoms (29%) before surgery. These possible mood dysfunctions are partly explained by tumor location. Severe depressive symptoms are associated with tumors in the right corticospinal tract, fornix, and inferior fronto-occipital fasciculus and the left uncinate fasciculus, whereas absence of depressive symptoms is associated with tumors in the left uncinate fasciculus and first segment of the superior longitudinal fasciculus and the right temporal cingulum and thalamus. Awareness of this phenomenon may be important for the identification of at-risk patients and patient counseling.

Methods

Patients

The study population consisted of 203 patients with a newly diagnosed supratentorial diffuse glioma included in several observational studies at the Amsterdam UMC location of Vrije Universiteit Amsterdam

https://doi.org/10.1038/s44220-024-00275-5

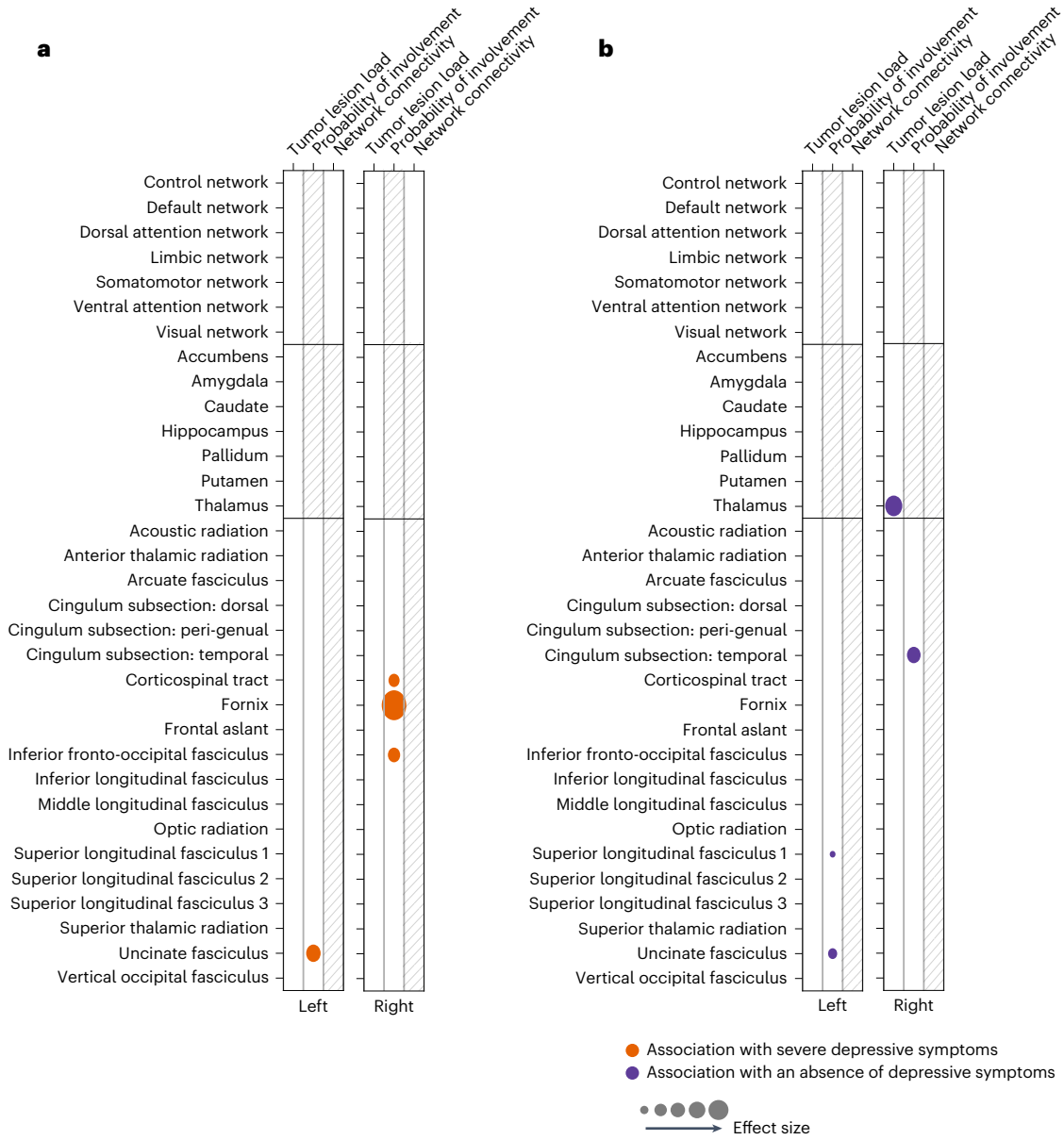

Fig. 5 | Overview of significant associations for each analysis. a, For severe depressive symptoms. **b**, For an absence of depressive symptoms. Bubble size corresponds with effect size.

between 2009 and 2022. All participants gave their informed consent for inclusion before study participation. Patients received no financial compensation for study participation. The study was conducted in accordance with the Declaration of Helsinki, the protocol was approved by the Medical Ethical Committee of the Amsterdam UMC location of Vrije Universiteit Amsterdam (2008.52; 2009.189; 2010.126; 2014.297), and all patients signed informed consent. We included patients of a combined sample that has partly been previously reported on[102]. This specific subpopulation and the MRIs have not been analyzed before. We followed the STROBE (Strengthening the Reporting of Observational Studies in Epidemiology) guidelines.

Inclusion criteria were patients who (1) were ≥18 years old, (2) had an MRI before surgery, (3) completed the CES-D within a year before surgery, and (4) had a histopathologic diagnosis of supratentorial diffuse glioma WHO (World Health Organization) 2016 grade II–IV following surgery. The MRI included at least a 3D T1-weighted scan without gadolinium (T1w) and a contrast-enhanced T1-weighted scan after gadolinium administration (T1c). If available, T2-weighted (T2w) and fluid attenuated inversion recovery (FLAIR)-weighted sequences were also collected. Only patients without a previous resection were included. Patients typically undergo several MRIs before surgery: initially when a lesion indicative of a diffuse glioma is suspected and again just before surgery to assist in procedural planning. Additional MRIs may be performed to monitor the lesion's progression. For the purpose of this study, we selected the preoperative MRI closest to the date of surgery for tumor segmentation.

We collected patient and tumor characteristics, including age, sex, handedness, educational level (low, middle, or high as classified according to the Verhage scale)[103], Karnofsky Performance Scale[104], SF-36 physical functioning subscale (higher scores represent better physical functioning)[105], whether patient had a history of a neuropsychiatric disease such as depression, information on the use of antiepileptic drugs or antidepressants, type of surgery (biopsy or resection), tumor grade and tumor type according to the WHO 2016 classification[1], and various time intervals: the time interval between first brain MRI with a lesion suspect for a diffuse glioma and CES-D measurement, the time

interval between the CES-D measurement and the preoperative MRI used for tumor segmentation, and the time interval between CES-D measurement and surgery. We categorized antiepileptic use into three groups: none, levetiracetam, and other antiepileptics, given the potential negative impact on mood from levetiracetam[106]. All patients had surgery as first cancer treatment, so radiotherapy and chemotherapy were not included as confounders in the analysis.

Statistics and reproducibility

This study combined data from multiple observational studies done at our institute. We combined these raw datasets and extracted variables and MRIs of interest (see the preceding paragraph), which had not been used for publication before. The MRIs were processed as described in Tumor locations. The MRIs were anonymized to ensure blinding during segmentation. No statistical method was used to predetermine sample size.

Depressive symptoms

Depressive symptoms were assessed with the CES-D, which is a widely used patient-reported outcome measure for depressive symptoms[100]. It has good validity and reliability in cancer patients and consists of 20 items about feelings and behaviors during the past week[107]. Scores for each item range from zero points (rarely or none of the time (less than 1 day)) to three points (all the time (5–7 days)), adding to a total score of 0–60. Higher scores indicate more depressive symptoms. We considered a score of ≥23 as severe depressive symptoms. An alternative cut-off of ≥21 yielded similar results in a sensitivity analysis. An overview of the number of patients per category can be found in Extended Data Tables 1–3.

Absence of depressive symptoms

A cut-off for an absence of depressive symptoms is lacking, therefore we based an arbitrary cut-off on several methods. First, as our population faced challenging circumstances, we expected some level of symptoms measured through the CES-D, that is, feeling fearful, restless sleep, decreased appetite, concentration difficulties, and/or feeling sad, similar to other newly diagnosed cancer patients. If patients scored the maximum three points for these five items, they would have a CES-D of at least 15. Conservatively, we decided half of these points (7.5, rounded conservatively to seven) would be a remarkable absence of depressive symptoms, especially considering the 15 other items on which patients could score additional points. Second, the mean CES-D score is eight to nine in the general population[108]. Third, we visually compared the CES-D distribution of our population with another newly diagnosed cancer population without intracranial metastases (Supplementary Fig. 1), consisting of 100 women who received a breast cancer stage 0–II diagnosis in the previous three months and were recruited for a psychoeducational intervention aimed at improving post-diagnosis distress[109]. In these patients also receiving a tumor diagnosis, 19% demonstrated a CES-D below 7, which is well below 29% and therefore corroborated our arbitrary cut-off.

Tumor locations

To determine tumor location, tumors were segmented using an automated nnU-Net algorithm[110] that can deal with missing pulse sequences followed by verification and manual editing (P.C.d.W.H., M.N.G.v.G., V.B.) under the supervision of an experienced neuroradiologist (F.B.) using 3D slicer v.5.0.2 (refs. 111,112). The segmentations included non-enhancing tumor parts from T2/FLAIR sequences combined with contrast-enhancing tumor parts and non-enhancing enclosed necrosis and cysts from T1w/T1c sequences. Segmentations were transformed from patient space (T1c) to Montreal Neurological Institute 152 standard space and resampled to 2 × 2 × 2 mm spatial resolution. Before transformation, skull stripping was performed using HD-BET brain extraction tool followed by a nonlinear registration with cost-function masking to standard space using ANTsPY v.0.3.2 (refs. 113,114). Tumor distribution maps in standard space were constructed by summing the tumor segmentations over all patients (Extended Data Fig. 1, upper right panel).

Disconnectome locations

The disconnectome represents white matter tracts likely affected by a (tumor) lesion. For each patient, a disconnectome was made using the BCBtoolkit v.4.2.0 (ref. 115). The BCBtoolkit creates disconnectomes from diffusion-weighted imaging data of 178 healthy subjects from the 7T Human Connectome Project[22,116]. In short, tumor segmentations in standard brain space were registered to each healthy participant's space using affine and diffeomorphic deformations[117,118]. The registered tumor segmentations were then used as seed for tractography in Trackvis for each healthy participant[119]. From the tractographies, a binary visitation map was constructed from each healthy participant for each patient, showing for each voxel whether it was intersected by a tract. Then the map was registered back to standard space and an averaged disconnectome was constructed for each patient from the visitation maps of all healthy participants. The resulting patient-specific disconnectome thus represents interindividual variability of tract reconstructions from healthy participants, with each voxel representing a probability of involvement ranging from 0 to 100%. To obtain the patient-specific binary disconnectome, we thresholded the disconnectome with a probability of 50% or more[115]. We then summed the binarized disconnectomes over all patients to create a structural disconnectome distribution map (Extended Data Fig. 1, upper right panel).

Lesion load analysis

The lesion load of tumors on specific brain structures was determined for each patient by considering parcels from standard brain atlases. The load was calculated as the tumor volume within a given parcel divided by the parcel's total volume. Three atlases were used: (1) the XTRACT probabilistic white matter atlases to define the subcortical white matter pathways using a tract probability of >0% to create binary tract masks, resulting in 41 tract structures[120], (2) Yeo's network atlas to define seven cortical parcels representing conjoined functional networks in each hemisphere, resulting in 14 cortical functional regions[121], and (3) the Harvard–Oxford atlas, resulting in 14 deep gray nuclei[122–125]. Similarly, disconnectome load on XTRACT white matter atlases was calculated.

Probability of involvement of white matter tracts

In addition, the probability of involvement—also known as the probability of disconnection—of a white matter tract by tumor location was determined by mapping the tumor lesions of each patient to XTRACT white matter atlases[120]. The probability was measured by determining the maximum probability of the tract crossing a tumor lesion using Tractotron software available in BCBtoolkit[115]. We considered a tract involved when the probability was larger than 0.5 (ref. 126).

Statistics

First, we determined the association between the CES-D category and the patient and tumor characteristics by applying a Bayesian categorical multiple regression model. We included age, sex, handedness, education level, antiepileptic drugs, SF-36 physical functioning subscale, tumor grade, tumor volume in milliliters, and the time interval between CES-D measurement and the first brain MRI with a suspected diffuse glioma (Extended Data Fig. 1, upper left panel). For six patients, the SF-36 questionnaire was missing. We used median interpolation of the SF-36 to include these patients in the model. The model with patient and tumor characteristics that were significantly associated with the CES-D category was considered the core model and used as the base for the following analysis.

The Bayesian regression model had vaguely informative priors as we had no specific prior knowledge on effect size of variables. The Markov chain Monte Carlo settings were at 2,000 draws and four

chains. The means of the posterior distributions were considered as estimates of the regression coefficients. Coefficients were considered statistically significant if the $HDI_{94\%}$ excluded zero. This threshold was originally chosen as a reminder that Bayesian credibility interval cut-offs are an arbitrary value determined by consensus. Models were generated and run using the PyMC package through the Bayesian model-building interface (Bambi) v.0.9.3 in python v.3.8.0 (ref. 127).

To determine the association between continuous CES-D scores and the locations of tumors and disconnectomes without assumptions on delineation of separate brain regions, we performed voxel-wise multivariate lesion symptom mapping using sparse canonical correlation analysis (SCCAN) (Extended Data Fig. 1, lower panel). This analysis was conducted using LESYMAP package v.0.0.0.9221 in R v.4.1.3 (ref. 128). The SCCAN method optimizes voxel weights that maximize the multivariate correlation between voxel values and CES-D scores. Fourfold within-sample cross-validation was used to evaluate the significance of the map. Using this method avoids some pitfalls associated with voxel-based methods as the significance of the entire map is tested at once[128]. We excluded voxels with fewer than three lesions.

To examine whether tumor or disconnectome load was related to CES-D category, we performed a Bayesian categorical regression as described in the preceding. The CES-D category was used as the dependent variable and tumor or disconnectome load per region for each of the specified atlases as independent variables, in addition to the core model (Extended Data Fig. 2, upper row).

To investigate whether white matter tract involvement was related to the CES-D category, we performed a categorical Bayesian regression with the involvements per tract as independent variables in addition to the core model (Extended Data Fig. 2, middle row).

Modeled functional network impact

We modeled potential tumor impact on functional networks by virtually lesioning normative functional network data according to patients' tumor locations. We utilized eigenvector centrality (EC) and local efficiency (LE) as graph theoretical measures to determine the importance of brain regions—regarded as nodes in the network[129]. The EC measures the importance of a node by the number of its own and its neighboring nodes' connections;[130] LE determines how connected the neighbors of a node are[131].

As a normative reference, we used processed[132] connectivity matrices of 1,000 publicly available Human Connectome Project participants. The matrices contain Pearson correlations that describe the pairwise correlations or co-activations between brain regions from resting-state functional MRIs. Brain regions consisted of 400 cortical parcels in Yeo's seven networks from the Schaefer surface atlas and 16 subcortical gray matter parcels from the Tian surface atlas[133,134]. We averaged all matrices to create a normative connectivity matrix and calculated graph measures LE and EC for each parcel (node) using the correlations as weights.

Next, using Freesurfer v.7.3.2 and Connectome Workbench v.1.5.0, we brought the tumor segmentations from volume to fsLR 32k surface space and overlaid these segmentations with the atlases to identify tumor-infiltrated brain region nodes. To create a synthetically lesioned matrix for each patient, we removed completely tumor-infiltrated parcels from the normative connectivity matrix and lowered the weights of partially tumor-infiltrated parcels according to the percentage of tumor load. We then calculated LE and EC for each remaining parcel of each patient and subtracted these from the normative matrix. To acquire the LE and EC difference of the seven networks due to the tumor, we calculated the median over all parcels within a network for each patient.

Finally, to determine the association between the CES-D category and modeled functional network impact, we used the median absolute graph measure differences in a Bayesian categorical regression. We performed a separate analysis for each measure, with the modeled difference measures of the seven networks as independent variables in addition to the core model (Extended Data Fig. 2, lower row).

Reporting summary

Further information on research design is available in the Nature Portfolio Reporting Summary linked to this article.

Data availability

XTRACT white matter atlases are freely available via GitHub (https://github.com/SPMIC-UoN/XTRACT_atlases). For WM tract atlases for the human (HCP and UK Biobank) and Macaque brain and connectivity blueprint atlases for the human (HCP) and macaque brain, we used HCP_tracts_1. Schaefer (and in turn Yeo) atlases are freely available via GitHub (https://github.com/ThomasYeoLab/CBIG/blob/master/stable_projects/brain_parcellation/Schaefer2018_LocalGlobal/Parcellations/Code/README.md). Harvard–Oxford atlases are freely available via Neurovault (https://neurovault.org/collections/262/). The Human Connectome Project processed connectivity matrices are freely available via Zenodo (https://zenodo.org/records/6770120)[135]. The primary patient dataset, including clinical variables and MRI scans, is not publicly available due to privacy regulations.

Code availability

All analysis packages and software used for data analysis throughout this manuscript are open source and freely available, thus not custom-made. R version 4.2.1 was used with the publicly available packages readxl, tidyverse, Hmisc, table1, and flextable. The LESYMAP package version 0.0.0.9221 is available via GitHub (https://github.com/dorianps/LESYMAP). The Bayesian model-building interface (Bambi) version 0.9.3 is available via GitHub (https://github.com/bambinos/bambi). ANTsX/ANTsPy: advanced normalization tools in Python version 0.3.2 is available via GitHub (https://github.com/ANTsX/ANTsPy). HD-BET: MRI brain extraction tool is available via GitHub (https://github.com/MIC-DKFZ/HD-BET). BCBtoolkit version 4.2.0 can be downloaded from www.bcblab.com. 3D Slicer version 5.0.2 can be downloaded from https://www.slicer.org/. Freesurfer version 7.3.2 can be downloaded from https://surfer.nmr.mgh.harvard.edu/. Connectome Workbench can be downloaded from https://www.humanconnectome.org/software/connectome-workbench.

References

1. Louis, D. N. et al. The 2016 World Health Organization Classification of Tumors of the Central Nervous System: a summary. *Acta Neuropathol.* **131**, 803–820 (2016).
2. Ostrom, Q. T., Cioffi, G., Waite, K., Kruchko, C. & Barnholtz-Sloan, J. S. CBTRUS statistical report: primary brain and other central nervous system tumors diagnosed in the United States in 2014–2018. *Neuro Oncol.* https://doi.org/10.1093/neuonc/noab200 (2021).
3. Boele, F. W., Klein, M., Reijneveld, J. C., Verdonck-de Leeuw, I. M. & Heimans, J. J. Symptom management and quality of life in glioma patients. *CNS Oncol.* **3**, 37–47 (2014).
4. Weller, M. et al. EANO guidelines on the diagnosis and treatment of diffuse gliomas of adulthood. *Nat. Rev. Clin. Oncol.* **18**, 170–186 (2021).
5. Stommel, M., Kurtz, M. E., Kurtz, J. C., Given, C. W. & Given, B. A. A longitudinal analysis of the course of depressive symptomatology in geriatric patients with cancer of the breast, colon, lung, or prostate. *Health Psychol.* **23**, 564–573 (2004).
6. Krebber, A. M. H. et al. Prevalence of depression in cancer patients: a meta-analysis of diagnostic interviews and self-report instruments. *Psychooncology.* **23**, 121–130 (2014).
7. Hu, Y. et al. Depression and quality of life in patients with gliomas: a narrative review. *J Clin. Med.* **11**, 4811 (2022).

8. Rooney, A. G., Carson, A. & Grant, R. Depression in cerebral glioma patients: a systematic review of observational studies. *J. Natl Cancer Inst.* **103**, 61–76 (2011).
9. Song, L. et al. Inflammation and behavioral symptoms in preoperational glioma patients: is depression, anxiety, and cognitive impairment related to markers of systemic inflammation? *Brain Behav.* **10**, e01771 (2020).
10. Campanella, F., Shallice, T., Ius, T., Fabbro, F. & Skrap, M. Impact of brain tumour location on emtion and personality: a voxel-based lesion–symptom mapping study on mentalization processes. *Brain* **137**, 2532–2545 (2014).
11. Boele, F. W., Rooney, A. G., Grant, R. & Klein, M. Psychiatric symptoms in glioma patients: from diagnosis to management. *Neuropsychiatr. Dis. Treat.* **11**, 1413–1420 (2015).
12. Lewandowska, A., Rudzki, G., Lewandowski, T. & Rudzki, S. The problems and needs of patients diagnosed with cancer and their caregivers. *Int. J. Environ. Res. Public Health* **18**, 87 (2021).
13. Christensen, M. C., Ren, H. & Fagiolini, A. Emotional blunting in patients with depression. Part II: relationship with functioning, well-being, and quality of life. *Ann. Gen. Psychiatry* **21**, 20 (2022).
14. Gläscher, J. et al. Lesion mapping of cognitive abilities linked to intelligence. *Neuron* **61**, 681–691 (2009).
15. Pisoni, A. et al. The neural correlates of auditory–verbal short-term memory: a voxel-based lesion–symptom mapping study on 103 patients after glioma removal. *Brain Struct. Funct.* **224**, 2199–2211 (2019).
16. Hendriks, E. J. et al. Linking late cognitive outcome with glioma surgery location using resection cavity maps. *Hum. Brain Mapp.* **39**, 2064–2074 (2018).
17. Bates, E. et al. Voxel-based lesion–symptom mapping. *Nat. Neurosci.* **6**, 448–450 (2003).
18. Gleichgerrcht, E., Fridriksson, J., Rorden, C. & Bonilha, L. Connectome-based lesion–symptom mapping (CLSM): a novel approach to map neurological function. *Neuroimage Clin.* **16**, 461–467 (2017).
19. Zhang, Y., Kimberg, D. Y., Coslett, H. B., Schwartz, M. F. & Wang, Z. Multivariate lesion–symptom mapping using support vector regression. *Hum. Brain Mapp.* **35**, 5861–5876 (2014).
20. Achilles, E. I. S. et al. Using multi-level Bayesian lesion–symptom mapping to probe the body-part-specificity of gesture imitation skills. *Neuroimage* **161**, 94–103 (2017).
21. Boes, A. D. et al. Network localization of neurological symptoms from focal brain lesions. *Brain* **138**, 3061–3075 (2015).
22. Thiebaut de Schotten, M., Foulon, C. & Nachev, P. Brain disconnections link structural connectivity with function and behaviour. *Nat. Commun.* **11**, 5094 (2020).
23. Salvalaggio, A., De Filippo De Grazia, M., Zorzi, M., Thiebaut de Schotten, M. & Corbetta, M. Post-stroke deficit prediction from lesion and indirect structural and functional disconnection. *Brain* **143**, 2173–2188 (2020).
24. Trapp, N. T. et al. Large-scale lesion symptom mapping of depression identifies brain regions for risk and resilience. *Brain* **146**, 1672–1685 (2023).
25. Weaver, N. A. et al. Strategic infarct locations for poststroke depressive symptoms: a lesion- and disconnection–symptom mapping study. *Biol. Psychiatry Cogn. Neurosci. Neuroimaging* **8**, 387–396 (2023).
26. Pan, C. et al. Neural substrates of poststroke depression: current opinions and methodology trends. *Front. Neurosci.* **16**, 812410 (2022).
27. van Grinsven, E. E. et al. The impact of etiology in lesion–symptom mapping—a direct comparison between tumor and stroke. *Neuroimage Clin.* **37**, 103305 (2023).
28. Leonetti, A. et al. Factors influencing mood disorders and health related quality of life in adults with glioma: a longitudinal study. *Front. Oncol.* **11**, 662039 (2021).
29. Bunevicius, A., Deltuva, V. P. & Tamasauskas, A. Association of pre-operative depressive and anxiety symptoms with five-year survival of glioma and meningioma patients: a prospective cohort study. *Oncotarget* **8**, 57543–57551 (2017).
30. Li, Y., Jin, Y., Wu, D. & Zhang, L. A depression network caused by brain tumours. *Brain Struct. Funct.* **227**, 2787–2795 (2022).
31. Arnold, S. D. et al. Evaluation and characterization of generalized anxiety and depression in patients with primary brain tumors. *Neuro Oncol.* **10**, 171–181 (2008).
32. Catani, M., Dell'Acqua, F. & Thiebaut de Schotten, M. A revised limbic system model for memory, emotion and behaviour. *Neurosci. Biobehav. Rev.* **37**, 1724–1737 (2013).
33. Conner, A. K. et al. A connectomic atlas of the human cerebrum—chapter 13: tractographic description of the inferior fronto-occipital fasciculus. *Oper. Neurosurg.* **15**, S436–S443 (2018).
34. Drevets, W. C., Price, J. L. & Furey, M. L. Brain structural and functional abnormalities in mood disorders: implications for neurocircuitry models of depression. *Brain Struct. Funct.* **213**, 93–118 (2008).
35. Hilland, E. et al. Exploring the links between specific depression symptoms and brain structure: a network study. *Psychiatry Clin. Neurosci.* **74**, 220–221 (2020).
36. Li, B. J. et al. A brain network model for depression: from symptom understanding to disease intervention. *CNS Neurosci. Ther.* **24**, 1004–1019 (2018).
37. Gray, J. P., Müller, V. I., Eickhoff, S. B. & Fox, P. T. Multimodal abnormalities of brain structure and function in major depressive disorder: a meta-analysis of neuroimaging studies. *Am. J. Psychiatry* **177**, 422–434 (2020).
38. Wijeratne, T. & Sales, C. Understanding why post-stroke depression may be the norm rather than the exception: the anatomical and neuroinflammatory correlates of post-stroke depression. *J. Clin. Med.* **10**, 1674 (2021).
39. Richey, L. N. et al. Neuroimaging correlates of syndromal depression following traumatic brain injury: a systematic review of the literature. *J. Concussion* **63**, 119–132 (2022).
40. Shen, Q. et al. Impaired white matter microstructure associated with severe depressive symptoms in patients with PD. *Brain Imaging Behav.* **16**, 169–175 (2022).
41. Elkommos, S. & Mula, M. A systematic review of neuroimaging studies of depression in adults with epilepsy. *Epilepsy Behav.* **115**, 107695 (2021).
42. Herbet, G., Yordanova, Y. N. & Duffau, H. Left spatial neglect evoked by electrostimulation of the right inferior fronto-occipital fasciculus. *Brain Topogr.* **30**, 747–756 (2017).
43. Herbet, G., Moritz-Gasser, S. & Duffau, H. Direct evidence for the contributive role of the right inferior fronto-occipital fasciculus in non-verbal semantic cognition. *Brain Struct. Funct.* **222**, 1597–1610 (2017).
44. Nys, G. M. S. et al. Early cognitive impairment predicts long-term depressive symptoms and quality of life after stroke. *J. Neurol. Sci.* **247**, 149–156 (2006).
45. Pan, C. et al. Structural disconnection-based prediction of poststroke depression. *Transl. Psychiatry* **12**, 461 (2022).
46. He, E. et al. White matter alterations in depressive disorder. *Front. Immunol.* **13**, 826812 (2022).
47. Turner, R. J. & Noh, S. Physical disability and depression: a longitudinal analysis. *J. Health Soc. Behav.* **29**, 23–37 (1988).
48. Bjelland, I. et al. Does a higher educational level protect against anxiety and depression? The HUNT study. *Soc. Sci. Med.* **66**, 1334–1345 (2008).

49. Schaepe, K. S. Bad news and first impressions: patient and family caregiver accounts of learning the cancer diagnosis. *Soc. Sci. Med.* **73**, 912–921 (2011).
50. Infurna, F. J., Gerstorf, D. & Ram, N. The nature and correlates of change in depressive symptoms with cancer diagnosis: reaction and adaptation. *Psychol. Aging* **28**, 386–401 (2013).
51. Vos, M. S., Putter, H., van Houwelingen, H. C. & de Haes, H. C. J. M. Denial in lung cancer patients: a longitudinal study. *Psychooncology* **17**, 1163–1171 (2008).
52. Vos, M. S., Putter, H., van Houwelingen, H. C. & de Haes, H. C. J. M. Denial and social and emotional outcomes in lung cancer patients: the protective effect of denial. *Lung Cancer* **72**, 119–124 (2011).
53. Andrewes, H. E., Drummond, K. J., Rosenthal, M., Bucknill, A. & Andrewes, D. G. Awareness of psychological and relationship problems amongst brain tumour patients and its association with carer distress. *Psychooncology* **22**, 2200–2205 (2013).
54. Starkstein, S. E., Jorge, R. E. & Robinson, R. G. The frequency, clinical correlates, and mechanism of anosognosia after stroke. *Can. J. Psychiatry* **55**, 355–361 (2010).
55. Starkstein, S. E., Fedoroff, J. P., Price, T. R., Leiguarda, R. & Robinson, R. G. Anosognosia in patients with cerebrovascular lesions: a study of causative factors. *Stroke.* **23**, 1446–1453 (1992).
56. Cocchini, G., Crosta, E., Allen, R., Zaro, F. & Beschin, N. Relationship between anosognosia and depression in aphasic patients. *J. Clin. Exp. Neuropsychol.* **35**, 337–347 (2013).
57. Conde-Sala, J. L. et al. Severity of dementia, anosognosia, and depression in relation to the quality of life of patients with Alzheimer disease: discrepancies between patients and caregivers. *Am. J. Geriatr. Psychiatry* **22**, 138–147 (2014).
58. Mograbi, D. C. & Morris, R. G. On the relation among mood, apathy, and anosognosia in Alzheimer's disease. *J. Int. Neuropsychol. Soc.* **20**, 2–7 (2014).
59. Yoo, H. S. et al. Cognitive anosognosia is associated with frontal dysfunction and lower depression in Parkinson's disease. *Eur. J. Neurol.* **27**, 951–958 (2020).
60. Le Heron, C., Apps, M. A. J. & Husain, M. The anatomy of apathy: a neurocognitive framework for amotivated behaviour. *Neuropsychologia* **118**, 54–67 (2018).
61. Hollocks, M. J. et al. Differential relationships between apathy and depression with white matter microstructural changes and functional outcomes. *Brain* **138**, 3803–3815 (2015).
62. Manca, R., Jones, S. A. & Venneri, A. Macrostructural and microstructural white matter alterations are associated with apathy across the clinical Alzheimer's disease spectrum. *Brain Sci.* **12**, 1383 (2022).
63. Steffens, D. C., Fahed, M., Manning, K. J. & Wang, L. The neurobiology of apathy in depression and neurocognitive impairment in older adults: a review of epidemiological, clinical, neuropsychological and biological research. *Transl. Psychiatry* **12**, 525 (2022).
64. Mulin, E. et al. Diagnostic criteria for apathy in clinical practice. *Int. J. Geriatr. Psychiatry.* **26**, 158–165 (2011).
65. Fahed, M. & Steffens, D. C. Apathy: neurobiology, assessment and treatment. *Clin. Psychopharmacol. Neurosci.* **19**, 181–189 (2021).
66. Miller, D. S. et al. Diagnostic criteria for apathy in neurocognitive disorders. *Alzheimers Dement.* **17**, 1892–1904 (2021).
67. Van Reekum, R., Donald, F. R. C. P. C., Stuss, T. L. & Ostrander, R. N. Apathy: why care? *J. Neuropsychiatry Clin. Neurosci.* **17**, 7–19 (2005).
68. Levy, R. & Dubois, B. Apathy and the functional anatomy of the prefrontal cortex-basal ganglia circuits. *Cereb. Cortex* **16**, 916–928 (2006).
69. Aubignat, M. et al. Poststroke apathy: major role of cognitive, depressive and neurological disorders over imaging determinants. *Cortex* **160**, 55–66 (2023).
70. Schei, S., Sagberg, L. M., Bø, L. E., Reinertsen, I. & Solheim, O. Association between patient-reported cognitive function and location of glioblastoma. *Neurosurg. Rev.* **46**, 282 (2023).
71. Hahn, C. et al. Apathy and white matter integrity in Alzheimer's disease: a whole brain analysis with tract-based spatial statistics. *PLoS ONE* **8**, e53493 (2013).
72. Powers, J. P. et al. White matter disease contributes to apathy and disinhibition in behavioral variant frontotemporal dementia. *Cogn. Behav. Neurol.* **27**, 206–214 (2014).
73. Setiadi, T. M. et al. Widespread white matter aberration is associated with the severity of apathy in amnestic mild cognitive impairment: tract-based spatial statistics analysis. *Neuroimage Clin.* **29**, 102567 (2021).
74. Bopp, M. H. A. et al. White matter integrity and symptom dimensions of schizophrenia: a diffusion tensor imaging study. *Schizophr. Res.* **184**, 59–68 (2017).
75. Whitford, T. J. et al. Localized abnormalities in the cingulum bundle in patients with schizophrenia: a diffusion tensor tractography study. *Neuroimage Clin.* **5**, 93–99 (2014).
76. Hoare, J. et al. White matter correlates of apathy in HIV-positive subjects: a diffusion tensor imaging study. *J. Neuropsychiatry Clin. Neurosci.* **22**, 313–320 (2010).
77. Rowland, L. M. et al. White matter alterations in deficit schizophrenia. *Neuropsychopharmacology* **34**, 1514–1522 (2009).
78. Nakajima, R., Kinoshita, M., Shinohara, H. & Nakada, M. The superior longitudinal fascicle: reconsidering the fronto-parietal neural network based on anatomy and function. *Brain Imaging Behav.* **14**, 2817–2830 (2020).
79. Padmanabhan, J. L. et al. A human depression circuit derived from focal brain lesions. *Biol. Psychiatry* **86**, 749–758 (2019).
80. Dean, J. & Keshavan, M. The neurobiology of depression: an integrated view. *Asian J. Psychiatry* **27**, 101–111 (2017).
81. Monje, M. Synaptic communication in brain cancer. *Cancer Res.* **80**, 2979–2982 (2020).
82. Bosma, I. et al. Disturbed functional brain networks and neurocognitive function in low-grade glioma patients: a graph theoretical analysis of resting-state MEG. *Nonlinear Biomed. Phys.* **3**, 9 (2009).
83. Derks, J. et al. Understanding global brain network alterations in glioma patients. *Brain Connect.* **11**, 865–974 (2021).
84. Hart, M. G., Romero-Garcia, R., Price, S. J. & Suckling, J. Global effects of focal brain tumors on functional complexity and network robustness: a prospective cohort study. *Neurosurgery* **84**, 1201–1213 (2019).
85. Numan, T. et al. Non-invasively measured brain activity and radiological progression in diffuse glioma. *Sci. Rep.* **11**, 18990 (2021).
86. Venkatesh, H. S. et al. Targeting neuronal activity-regulated neuroligin-3 dependency in high-grade glioma. *Nature* **549**, 533–537 (2017).
87. Venkataramani, V. et al. Glutamatergic synaptic input to glioma cells drives brain tumour progression. *Nature* **573**, 532–538 (2019).
88. Cuddapah, V. A., Robel, S., Watkins, S. & Sontheimer, H. A neurocentric perspective on glioma invasion. *Nat. Rev. Neurosci.* **15**, 455–465 (2014).
89. Venkatesh, H. S. et al. Electrical and synaptic integration of glioma into neural circuits. *Nature.* **573**, 539–545 (2019).
90. Krishna, S. et al. Glioblastoma remodelling of human neural circuits decreases survival. *Nature* **617**, 599–607 (2023).

91. Traut, T. et al. MEG imaging of recurrent gliomas reveals functional plasticity of hemispheric language specialization. *Hum. Brain Mapp.* **40**, 1082–1092 (2019).
92. Guggisberg, A. G. et al. Mapping functional connectivity in patients with brain lesions. *Ann. Neurol.* **63**, 193–203 (2008).
93. Seghier, M. L. The elusive metric of lesion load. *Brain Struct. Funct.* **228**, 703–716 (2023).
94. Hope, T. M. H., Seghier, M. L., Prejawa, S., Leff, A. P. & Price, C. J. Distinguishing the effect of lesion load from tract disconnection in the arcuate and uncinate fasciculi. *Neuroimage* **125**, 1169–1173 (2016).
95. Joutsa, J., Corp, D. T. & Fox, M. D. Lesion network mapping for symptom localization: recent developments and future directions. *Curr. Opin. Neurol.* **35**, 453–459 (2022).
96. Duffau, H. Diffuse low-grade gliomas and neuroplasticity. *Diagn. Interv. Imaging* **95**, 945–955 (2014).
97. Kong, N. W., Gibb, W. R. & Tate, M. C. Neuroplasticity: insights from patients harboring gliomas. *Neural Plast.* **2016**, 2365063 (2016).
98. Visser, M. et al. Inter-rater agreement in glioma segmentations on longitudinal MRI. *Neuroimage Clin.* **22**, 101727 (2019).
99. Visser, M. et al. Accurate MR image registration to anatomical reference space for diffuse glioma. *Front. Neurosci.* **14**, 585 (2020).
100. Radloff, L. S. The CES-D scale: a self-report depression scale for research in the general population. *Appl. Psychol. Meas.* **1**, 385–401 (1977).
101. Sekely, A. et al. Neurocognitive impairment, neurobehavioral symptoms, fatigue, sleep disturbance, and depressive symptoms in patients with newly diagnosed glioblastoma. *Neurooncol. Pract.* **10**, 89–96 (2022).
102. Röttgering, J. G. et al. Symptom networks in glioma patients: understanding the multidimensionality of symptoms and quality of life. *J Cancer Surviv.* **18**, 1032–1041 (2023).
103. Verhage, F. *Intelligentie en leeftijd onderzoek bij Nederlanders van twaalf tot zevenenzeventig jaar* (Van Gorcum, 1964).
104. Schag, C. C., Heinrich, R. L. & Ganz, P. A. Karnofsky performance status revisited: reliability, validity, and guidelines. *J. Clin. Oncol.* **2**, 187–193 (1984).
105. Ware, J. E. J. & Sherbourne, C. D. The MOS 36-item short-form health survey (SF-36). I. Conceptual framework and item selection. *Med. Care.* **30**, 473–483 (1992).
106. Chen, B. et al. Psychiatric and behavioral side effects of antiepileptic drugs in adults with epilepsy. *Epilepsy Behav.* **76**, 24–31 (2017).
107. Hann, D., Winter, K. & Jacobsen, P. Measurement of depressive symptoms in cancer patients: evaluation of the Center for Epidemiological Studies Depression Scale (CES-D). *J. Psychosom. Res.* **46**, 437–443 (1999).
108. Bouma, J., Ranchor, A. V., Sanderman, R. & van Sonderen, E. *Het meten van symptomen van depressie met de CES-D: Een handleiding* (Noordelijk Centrum voor Gezondheidsvraagstukken, Rijksuniversiteit Groningen, 1995).
109. Lally, R. M. et al. CaringGuidance™ after breast cancer diagnosis eHealth psychoeducational intervention to reduce early post-diagnosis distress. *Support. Care Cancer* **28**, 2163–2174 (2020).
110. Pemberton, H.G. et al. Multi-class glioma segmentation on real-world data with missing MRI sequences: comparison of three deep learning algorithms. *Sci. Rep.* **13**, 18911 (2023).
111. Kikinis, R., Pieper, S. D., Vosburgh, K. G. in *Intraoperative Imaging and Image-Guided Therapy* (ed. Jolesz, F. A.) 277–289 (Springer, 2014); https://doi.org/10.1007/978-1-4614-7657-3_19
112. Fedorov, A. et al. 3D Slicer as an image computing platform for the quantitative imaging network. *Magn. Reson. Imaging* **30**, 1323–1341 (2012).
113. Avants, B. B., Epstein, C. L., Grossman, M. & Gee, J. C. Symmetric diffeomorphic image registration with cross-correlation: evaluating automated labeling of elderly and neurodegenerative brain. *Med. Image Anal.* **12**, 26–41 (2008).
114. Isensee, F. et al. Automated brain extraction of multisequence MRI using artificial neural networks. *Hum. Brain Mapp.* **40**, 4952–4964 (2019).
115. Foulon, C. et al. Advanced lesion symptom mapping analyses and implementation as BCBtoolkit. *Gigascience* https://doi.org/10.1093/gigascience/giy004 (2018).
116. Vu, A. T. et al. High resolution whole brain diffusion imaging at 7T for the Human Connectome Project. *Neuroimage* **122**, 318–331 (2015).
117. Klein, A. et al. Evaluation of 14 nonlinear deformation algorithms applied to human brain MRI registration. *Neuroimage* **46**, 786–802 (2009).
118. Avants, B. B. et al. A reproducible evaluation of ANTs similarity metric performance in brain image registration. *Neuroimage* **54**, 2033–2044 (2011).
119. Wang, R. & Benner, T. Diffusion toolkit: a software package for diffusion imaging data processing and tractography. *Proc. Intl Soc. Magn. Reson. Med.* **15**, 3720 (2007).
120. Warrington, S. et al. XTRACT—standardised protocols for automated tractography in the human and macaque brain. *Neuroimage* **217**, 116923 (2020).
121. Thomas Yeo, B. T. et al. The organization of the human cerebral cortex estimated by intrinsic functional connectivity. *J. Neurophysiol.* **106**, 1125–1165 (2011).
122. Makris, N. et al. Decreased volume of left and total anterior insular lobule in schizophrenia. *Schizophr. Res.* **83**, 155–171 (2006).
123. Frazier, J. A. et al. Structural brain magnetic resonance imaging of limbic and thalamic volumes in pediatric bipolar disorder. *Am. J. Pyschiatry* **162**, 1256–1265 (2005).
124. Desikan, R. S. et al. An automated labeling system for subdividing the human cerebral cortex on MRI scans into gyral based regions of interest. *Neuroimage.* **31**, 968–980 (2006).
125. Goldstein, J. M. et al. Hypothalamic abnormalities in schizophrenia: sex effects and genetic vulnerability. *Biol. Psychiatry* **61**, 935–945 (2007).
126. Thiebaut De Schotten, M. et al. Damage to white matter pathways in subacute and chronic spatial neglect: a group study and 2 single-case studies with complete virtual 'in vivo' tractography dissection. *Cereb. Cortex* **24**, 691–706 (2014).
127. Capretto, T. et al. Bambi: a simple interface for fitting Bayesian linear models in Python. *J. Stat. Softw.* https://doi.org/10.18637/jss.v103.i15 (2022).
128. Pustina, D., Avants, B., Faseyitan, O. K., Medaglia, J. D. & Coslett, H. B. Improved accuracy of lesion to symptom mapping with multivariate sparse canonical correlations. *Neuropsychologia* **115**, 154–166 (2018).
129. Gervini Zampieri Centeno, E., Moreni, G., Vriend, C., Douw, L. & Nóbrega Santos, A. A hands-on tutorial on network and topological neuroscience. *Brain Struct. Funct.* **227**, 741–762 (2021).
130. Golbeck, J. in *Analyzing the Social Web* (ed. Golbeck, J.) 25–44 (Morgan Kaufmann, 2013); https://doi.org/10.1016/B978-0-12-405531-5.00003-1
131. Latora, V. & Marchiori, M. Efficient behavior of small-world networks. *Phys. Rev. Lett.* **87**, 198701 (2001).
132. Tijhuis, F. et al. Human Connectome project rfMRI repository. *GitHub* https://github.com/floristijhuis/HCP-rfMRI-repository (2023).
133. Schaefer, A. et al. Local–global parcellation of the human cerebral cortex from intrinsic functional connectivity MRI. *Cereb. Cortex* **28**, 3095–3114 (2018).
134. Tian, Y., Margulies, D. S., Breakspear, M. & Zalesky, A. Topographic organization of the human subcortex unveiled with functional connectivity gradients. *Nat. Neurosci.* **23**, 1421–1432 (2020).

135. Tijhuis, F. B. et al. Human connectome project resting-state fMRI connectivity matrices (young adult + aging). *Zenodo* https://zenodo.org/doi/10.5281/zenodo.6770119 (2022).

Acknowledgments

We thank R. M. Lally and K. A. Kupzyk, both affiliated with the College of Nursing, University of Nebraska Medical Center, Omaha, NE, USA, for sharing their data. This project is funded by a grant for public–private partnerships (Amsterdam UMC PPP-grant) sponsored by the Dutch government through the Rijksdienst voor Ondernemend Nederland and Topsector Life Sciences and Health, 'Picturing predictions for patients with brain tumors' (M.N.G.v.G., R.S.E., P.C.d.W.H.); the Anita Veldman Foundation, CCA2018-2-17 (V.B., J.M.N., L.D., J.G.R., M.G., M.E.C.B., M.K., P.C.d.W.H.), and the National Institute for Health Research (NIHR) biomedical research center at UCLH (F.B.).

Author contributions

All authors commented on previous drafts and approved the final paper. The conceptualization of the project was done by M.N.G.v.G., V.B., L.D., R.S.E. and P.C.d.W.H. Data collection was carried out by L.D. and M.K. Segmentation was performed by M.N.G.v.G., V.B. and P.C.d.W.H. Analyses were conducted by M.N.G.v.G., V.B. and R.S.E. The first draft of the paper was written by M.N.G.v.G. and V.B. Review and editing of the paper were done by J.M.N., L.D., J.G.R., M.G., M.E.C.B., F.B., M.K., R.S.E. and P.C.d.W.H. Supervision was provided by J.M.N., F.B., R.S.E. and P.C.d.W.H.

Competing interests

The authors declare no competing interests.

Additional information

Extended data is available for this paper at https://doi.org/10.1038/s44220-024-00275-5.

Supplementary information The online version contains supplementary material available at https://doi.org/10.1038/s44220-024-00275-5.

Correspondence and requests for materials should be addressed to Philip C. De Witt Hamer.

Peer review information *Nature Mental Health* thanks Nicholas Trapp, Frank Winkler, and the other, anonymous, reviewer(s) for their contribution to the peer review of this work.

https://doi.org/10.1038/s44220-024-00275-5

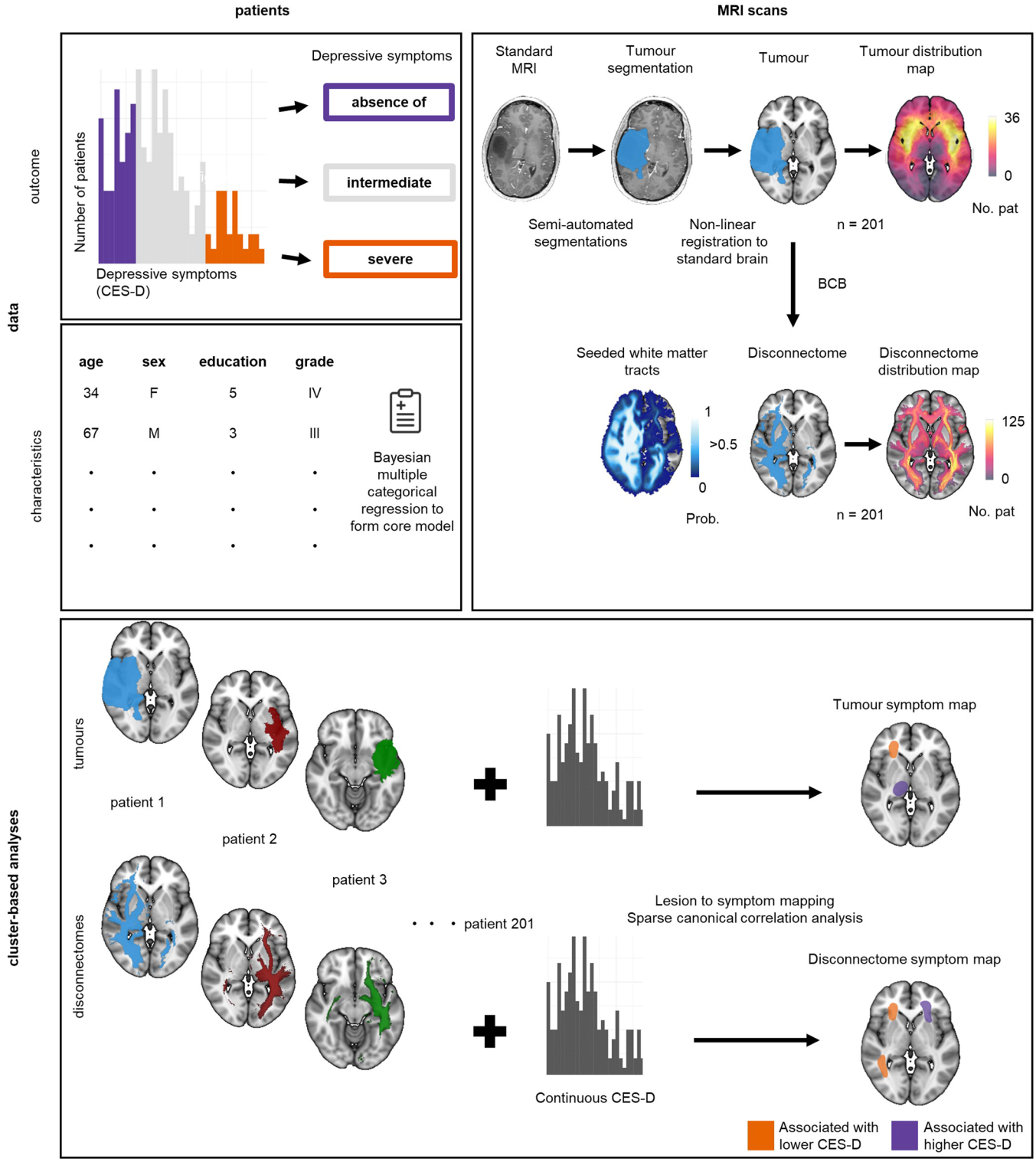

Extended Data Fig. 1 | Overview of methods: data and cluster-based analyses. ***Data***, Patients' raw CES-D scores were split into three categories: an absence of (≤6; ADS), intermediate (7-22) and severe (≥23; SDS) depressive symptoms. We tested which patient and tumor characteristics were significantly associated with the CES-D category as core model using a Bayesian categorical multiple regression. Structural ***MRI scans*** were utilized to create semi-automated segmentations followed by a non-linear registration to MNI152 standard space. With the segmentations we constructed **a**) tumor distribution maps of all patients and **b**) patient-specific disconnectomes and disconnectome distribution maps of all patients. ***Cluster-based analyses***. Patients' tumor segmentations (T) and continuous CES-D scores were used as input for lesion to symptom mapping with sparse canonical correlation analysis. This resulted in a tumor symptom map with clusters of voxels corresponding to either severe or an absence of depressive symptoms. Accordingly, disconnectomes and continuous CES-D scores were used as input for a disconnectome symptom map.

https://doi.org/10.1038/s44220-024-00275-5

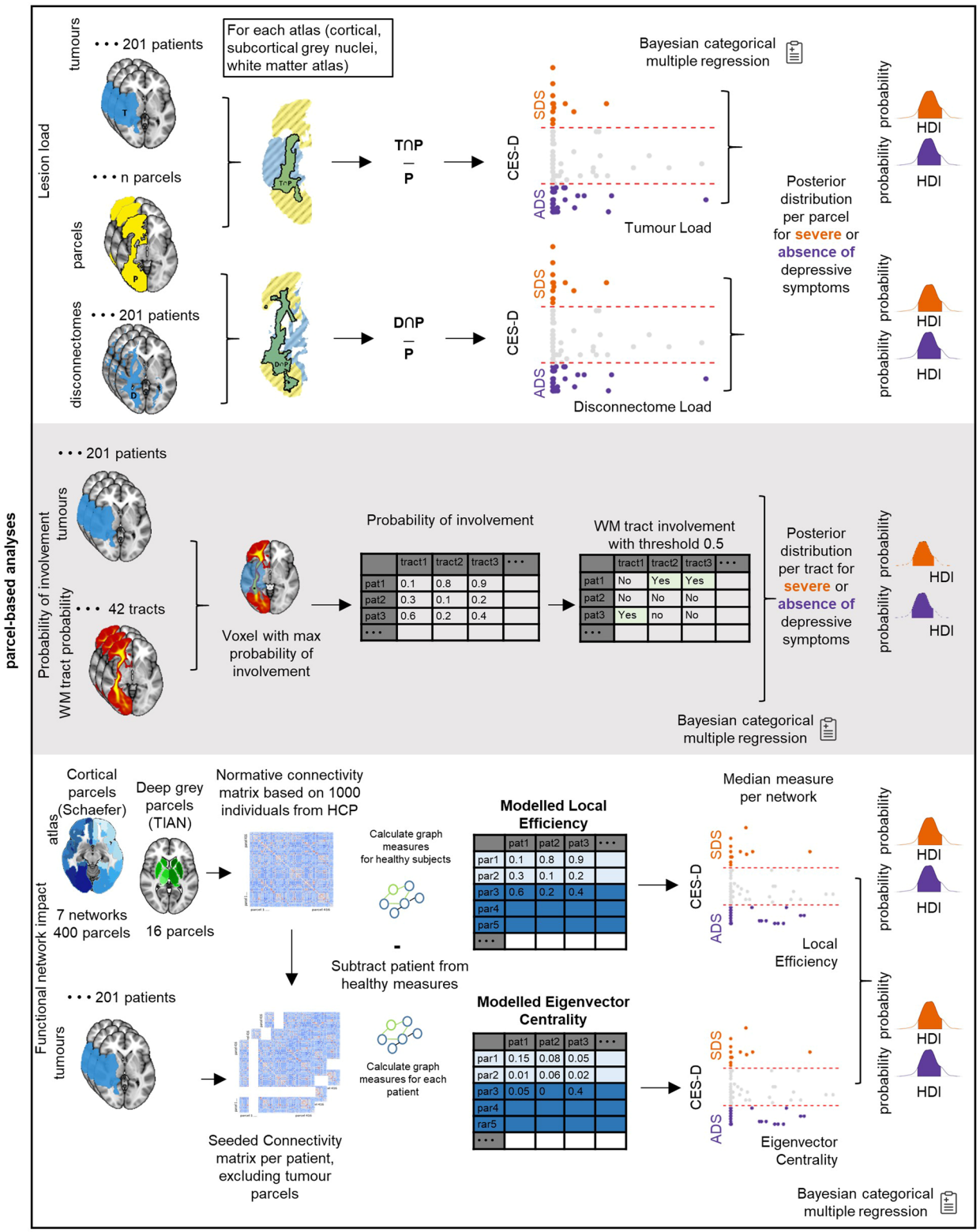

	tract1	tract2	tract3	• • •
pat1	0.1	0.8	0.9	
pat2	0.3	0.1	0.2	
pat3	0.6	0.2	0.4	
• • •				

	tract1	tract2	tract3	• • •
pat1	No	Yes	Yes	
pat2	No	No	No	
pat3	Yes	no	No	
• • •				

	pat1	pat2	pat3	• • •
par1	0.1	0.8	0.9	
par2	0.3	0.1	0.2	
par3	0.6	0.2	0.4	
par4				
par5				
• • •				

	pat1	pat2	pat3	• • •
par1	0.15	0.08	0.05	
par2	0.01	0.06	0.02	
par3	0.05	0	0.4	
par4				
rar5				
• • •				

Extended Data Fig. 2 | See next page for caption.

https://doi.org/10.1038/s44220-024-00275-5

Extended Data Fig. 2 | Overview of methods: parcel-based analyses. ***Parcel-based analyses of lesion load***. To calculate lesion load per patient per parcel, overlapping tumor-parcel volumes (T∩P) were calculated and divided by total parcel volumes (P). Hence, to examine associations with the CES-D category, these lesion loads, patient and tumor characteristics were analysed with Bayesian categorical multiple regression. This resulted in posterior distributions of a regression coefficient per parcel for both SDS and ADS with highest density interval (HDI). This step was repeated for all parcels of all three atlases (Yeo's network atlas for cortical regions, Harvard-Oxford for subcortical grey nuclei, XTRACT for white matter tracts). Additionally, we repeated the analysis for disconnectome (D) load on XTRACT atlases. ***Probability of involvement*** was calculated by determining the maximum probability of the tract crossing a tumor using BCBToolkit[55]. Tract involvement was defined as a probability of involvement >0.5. Associations with CES-D category were analysed with Bayesian categorical multiple regression. ***Functional network impact***. We constructed a normative connectivity matrix of local efficiency (LE) and eigenvector centrality (EC) for Schaefer and Tian parcellations. We overlaid tumor segmentations with these parcels to determine the tumor-infiltrated parcels and model patient-specific connectivity matrices by excluding these completely tumor-infiltrated parcels or lowering the weights of partially-infiltrated parcels accordingly. We then calculated LE and EC for each brain region for every patient and subtracted these from the normative values. The median of these differences was calculated over parcels belonging to each specific network. The modelled median differences for each network per graph measure were then analysed with Bayesian categorical regression including significant patient and tumor characteristics.

https://doi.org/10.1038/s44220-024-00275-5

Extended Data Table 1 | Patient characteristics overall and per depressive symptom category

	Overall (N=201)	Depressive symptoms		
		Absence of (N=59)	Intermediate (N=113)	Severe (N=29)
Age				
Median [IQR]	46.0 [23.0]	42.0 [25.0]	48.0 [21.0]	47.0 [22.0]
Sex				
Female	77 (38.3%)	18 (30.5%)	41 (36.3%)	18 (62.1%)
Handedness				
Right	172 (85.6%)	48 (81.4%)	97 (85.8%)	27 (93.1%)
Left	19 (9.5%)	6 (10.2%)	11 (9.7%)	2 (6.9%)
Ambidexter	10 (5.0%)	5 (8.5%)	5 (4.4%)	0 (0%)
Level of education (Verhage)				
Low (1-4)	44 (21.9%)	9 (15.3%)	25 (22.1%)	10 (34.5%)
Middle (5)	61 (30.3%)	12 (20.3%)	37 (32.7%)	12 (41.4%)
High (6-7)	96 (47.8%)	38 (64.4%)	51 (45.1%)	7 (24.1%)
KPS				
<70	3 (1.5%)	0 (0%)	2 (1.8%)	1 (3.4%)
70-80	20 (10.0%)	3 (5.1%)	13 (11.5%)	4 (13.8%)
90-100	147 (73.1%)	46 (78.0%)	80 (70.8%)	21 (72.4%)
Missing	31 (15.4%)	10 (16.9%)	18 (15.9%)	3 (10.3%)
SF-36, Physical functioning				
Median [IQR]	90.0 [20.0]	100 [10.0]	90.0 [20.0]	70.0 [25.0]
Missing	6 (3.0%)	2 (3.4%)	2 (1.8%)	2 (6.9%)
History of neuropsychiatric disease				
No	189 (94.0%)	58 (98.3%)	106 (93.8%)	25 (86.2%)
Depression	4 (2.0%)	0 (0%)	3 (2.7%)	1 (3.4%)
Other	8 (4.0%)	1 (1.7%)	4 (3.5%)	3 (10.3%)
Use of antidepressants				
No	195 (97.0%)	58 (98.3%)	110 (97.3%)	27 (93.1%)
Yes	6 (3.0%)	1 (1.7%)	3 (2.7%)	2 (6.9%)

IQR Interquartile range; *KPS* Karnofsky Performance Scale; *SF-36* Short Form-36

https://doi.org/10.1038/s44220-024-00275-5

Extended Data Table 2 | Tumour characteristics overall and per depressive symptom category

	Overall (N=201)	Depressive symptoms		
		Absence of (N=59)	Intermediate (N=113)	Severe (N=29)
Hemisphere				
Left	115 (57.2%)	35 (59.3%)	62 (54.9%)	18 (62.1%)
Right	83 (41.3%)	23 (39.0%)	49 (43.4%)	11 (37.9%)
Both	3 (1.5%)	1 (1.7%)	2 (1.8%)	0 (0%)
Histology				
Oligodendroglioma	66 (32.8%)	17 (28.8%)	37 (32.7%)	12 (41.4%)
Oligoastrocytoma*	8 (4.0%)	2 (3.4%)	5 (4.4%)	1 (3.4%)
Astrocytoma	70 (34.8%)	28 (47.5%)	32 (28.3%)	10 (34.5%)
Glioblastoma	57 (28.4%)	12 (20.3%)	39 (34.5%)	6 (20.7%)
IDH status				
Mutated	100 (49.8%)	34 (57.6%)	53 (46.9%)	13 (44.8%)
Wildtype	44 (21.9%)	10 (16.9%)	28 (24.8%)	6 (20.7%)
Unknown	57 (28.4%)	15 (25.4%)	32 (28.3%)	10 (34.5%)
1p19q status				
1p loss	2 (1.0%)	0 (0%)	2 (1.8%)	0 (0%)
Codeleted	59 (29.4%)	17 (28.8%)	32 (28.3%)	10 (34.5%)
No deletion	55 (27.4%)	21 (35.6%)	24 (21.2%)	10 (34.5%)
Unknown	85 (42.3%)	21 (35.6%)	55 (48.7%)	9 (31.0%)
Grade				
II	91 (45.3%)	33 (55.9%)	44 (38.9%)	14 (48.3%)
III	52 (25.9%)	14 (23.7%)	30 (26.5%)	8 (27.6%)
IV	58 (28.9%)	12 (20.3%)	39 (34.5%)	7 (24.1%)
Tumour volume (ml)				
Median [IQR]	64.1 [78.2]	54.7 [55.5]	67.3 [88.3]	48.1 [45.4]

*As defined by the WHO 2007 classification

IQR Interquartile range

https://doi.org/10.1038/s44220-024-00275-5

Extended Data Table 3 | Treatment and timing characteristics overall and per depressive symptom category

	Overall (N=201)	Depressive symptoms		
		Absence of (N=59)	Intermediate (N=113)	Severe (N=29)
Use of antiepileptics				
None	45 (22.4%)	15 (25.4%)	27 (23.9%)	3 (10.3%)
Yes, including levetiracetam	108 (53.7%)	30 (50.8%)	58 (51.3%)	20 (69.0%)
Yes, other than levetiracetam	48 (23.9%)	14 (23.7%)	28 (24.8%)	6 (20.7%)
Surgery type				
Resection	187 (93.0%)	55 (93.2%)	105 (92.9%)	27 (93.1%)
Biopsy	14 (7.0%)	4 (6.8%)	8 (7.1%)	2 (6.9%)
Time interval between CES-D and preoperative MRI used for tumour segmentation in weeks				
Median [IQR]	0.43 [4.0]	0.29 [6.14]	0.43 [3.43]	0.29 [4.14]
Time interval between CES-D and surgery in weeks				
Median [IQR]	3.14 [7.57]	4.57 [8.79]	2.57 [6.57]	2.86 [6.14]
Time interval between first MRI and CES-D in weeks				
Median [IQR]	10.6 [17.3]	10.0 [21.4]	10.4 [13.6]	10.7 [17.4]

CES-D Center for Epidemiologic Studies Depression Scale; *IQR* Interquartile range

nature portfolio

Corresponding author(s): Philip de Witt Hamer

Last updated by author(s): May 13, 2024

Reporting Summary

Nature Portfolio wishes to improve the reproducibility of the work that we publish. This form provides structure for consistency and transparency in reporting. For further information on Nature Portfolio policies, see our Editorial Policies and the Editorial Policy Checklist.

Statistics

For all statistical analyses, confirm that the following items are present in the figure legend, table legend, main text, or Methods section.

n/a	Confirmed	
☐	☒	The exact sample size (*n*) for each experimental group/condition, given as a discrete number and unit of measurement
☐	☒	A statement on whether measurements were taken from distinct samples or whether the same sample was measured repeatedly
☒	☐	The statistical test(s) used AND whether they are one- or two-sided *Only common tests should be described solely by name; describe more complex techniques in the Methods section.*
☐	☒	A description of all covariates tested
☐	☒	A description of any assumptions or corrections, such as tests of normality and adjustment for multiple comparisons
☐	☒	A full description of the statistical parameters including central tendency (e.g. means) or other basic estimates (e.g. regression coefficient) AND variation (e.g. standard deviation) or associated estimates of uncertainty (e.g. confidence intervals)
☒	☐	For null hypothesis testing, the test statistic (e.g. *F*, *t*, *r*) with confidence intervals, effect sizes, degrees of freedom and *P* value noted *Give P values as exact values whenever suitable.*
☐	☒	For Bayesian analysis, information on the choice of priors and Markov chain Monte Carlo settings
☒	☐	For hierarchical and complex designs, identification of the appropriate level for tests and full reporting of outcomes
☐	☒	Estimates of effect sizes (e.g. Cohen's *d*, Pearson's *r*), indicating how they were calculated

Our web collection on statistics for biologists contains articles on many of the points above.

Software and code

Policy information about availability of computer code

Data collection	Data was collected prior to our study; we did therefore not use any software for data collection.
Data analysis	For merging of datasets, data cleaning and making tables and histograms, R version 4.2.1 was used with the publicly available packages "readxl", "tidyverse", "Hmisc", "table1", and "flextable". Data was further analysed using the LESYMAP package version 0.0.0.9221 available in R of which we used version 4.1.3 and PyMC package through the Bayesian model building interface (Bambi) version 0.9.3 available in python of which we used version 3.8. Additionally, for image processing we used 3D slicer, version 5.0.2, ANTsPY version 0.3.2, HD-BET git commit ea49413, BCBtoolkit version 4.2.0 and freesurfer version 7.3.2

For manuscripts utilizing custom algorithms or software that are central to the research but not yet described in published literature, software must be made available to editors and reviewers. We strongly encourage code deposition in a community repository (e.g. GitHub). See the Nature Portfolio guidelines for submitting code & software for further information.

Data

Policy information about availability of data

All manuscripts must include a data availability statement. This statement should provide the following information, where applicable:

- Accession codes, unique identifiers, or web links for publicly available datasets
- A description of any restrictions on data availability
- For clinical datasets or third party data, please ensure that the statement adheres to our policy

XTRACT white matter atlases are freely available from: GitHub - SPMIC-UoN/XTRACT_atlases: WM tract atlases for the human (HCP and UK Biobank) and Macaque brain and connectivity blueprint atlases for the human (HCP) and macaque brain., we used HCP_tracts_1. Schaefer (and in turn Yeo) atlases are freely available from: CBIG/stable_projects/brain_parcellation/Schaefer2018_LocalGlobal at master · ThomasYeoLab/CBIG · GitHub. Harvard-Oxford atlases are freely available from: Harvard-Oxford cortical and subcortical structural atlases (neurovault.org). The human connectome project processed connectivity matrices are freely available from: Human Connectome Project resting-state fMRI Connectivity Matrices (Young Adult + Aging) (zenodo.org). The primary patient dataset including clinical variables and MRI scans are not publicly available due to privacy regulations.

Research involving human participants, their data, or biological material

Policy information about studies with human participants or human data. See also policy information about sex, gender (identity/presentation), and sexual orientation and race, ethnicity and racism.

Reporting on sex and gender	We included both sexes in this study and sex was a significant factor in our analysis. Sex was collected from hospital systems which was based on official government issued identification. Out of 201 patients, 77 (38%) had the female sex. We do not report on gender.
Reporting on race, ethnicity, or other socially relevant groupings	There was no social grouping. We do report on patients educational level (Verhage scale). Patients self-reported on their education and were then further classified into either of three Verhage categories; low, middle or high.
Population characteristics	As covariates we considered: age (median age 46 years), sex (38.3% female), handedness (85.6% right-handed), education level (47.8% high education, 30.3% middle education), SF-36 physical functioning (median 90), history of epileptics (53.7% yes, including levetiracetam and 23.9% yes, other than levetiracetam), tumour grade (45.3% grade II, 25.9% grade III), tumour volume in ml and the time interval between CES-D measurment and first brain MRI with a suspected diffuse glioma (median 10.6 weeks).
Recruitment	Patients were recruited through outpatient visit when suspected for a diffuse glioma. Only patients with sufficient capacity to provide informed consent and fill out the questionnaires were recruited which may introduce subject bias.
Ethics oversight	The Medical Ethical Committee of Amsterdam UMC location Vrije Universiteit Amsterdam approved the study protocols.

Note that full information on the approval of the study protocol must also be provided in the manuscript.

Field-specific reporting

Please select the one below that is the best fit for your research. If you are not sure, read the appropriate sections before making your selection.

☒ Life sciences ☐ Behavioural & social sciences ☐ Ecological, evolutionary & environmental sciences

For a reference copy of the document with all sections, see nature.com/documents/nr-reporting-summary-flat.pdf

Life sciences study design

All studies must disclose on these points even when the disclosure is negative.

Sample size	We did not perform any sample size calculations. The sample size was reached through selecting patients that met the inclusion criteria from different observational studies between 2009 and 2022 which we previously reported on.
Data exclusions	Two patients were excluded from the sample due to poor registration of their MRI images to standard brain space.
Replication	We did not replicate measurements. We analyze an observational cohort which was previously analyzed for different research questions.
Randomization	Patients were not allocated to experimental groups, thus not randomized.
Blinding	Patients were not allocated to experimental groups, thus no blinding was necessary.

Reporting for specific materials, systems and methods

We require information from authors about some types of materials, experimental systems and methods used in many studies. Here, indicate whether each material, system or method listed is relevant to your study. If you are not sure if a list item applies to your research, read the appropriate section before selecting a response.

Materials & experimental systems

n/a	Involved in the study
☒	☐ Antibodies
☒	☐ Eukaryotic cell lines
☒	☐ Palaeontology and archaeology
☒	☐ Animals and other organisms
☒	☐ Clinical data
☒	☐ Dual use research of concern
☒	☐ Plants

Methods

n/a	Involved in the study
☒	☐ ChIP-seq
☒	☐ Flow cytometry
☐	☒ MRI-based neuroimaging

Magnetic resonance imaging

Experimental design

Design type	n/a
Design specifications	n/a
Behavioral performance measures	n/a

Acquisition

Imaging type(s)	Structural data from routine clinical imaging
Field strength	1.5T
Sequence & imaging parameters	We included a non contrast enhances axial T1-weighted spin echo image with TR/TE 520-600/8-12 ms with 5mm slice thickness, a gadolinium enhanced sagittal 3D T1-weighted gradient-echo image (MPRAGE, TR/TE/TI 2300-2700/5-4.5/95 ms) with 1-1.5mm slice thickness, an axial T2-weighted turbo spin echo image (TR/TE 5190-8670/93-101 ms) with 5mm slice thickness, and sagittal 3D turbo fluid-attenuated inversion-recorvery (FLAIR) image (TR/TE/TE 6500/355/2200 ms) with 1.3mm slice thickness.
Area of acquisition	whole brain

Diffusion MRI ☐ Used ☒ Not used

Preprocessing

Preprocessing software	We used an in-house developed nn-Unet segmentation algorithm and manually verified these segmentations in 3D slicer version 5.0.2. The segmentations included non-enhancing tumour parts from T2/FLAIR sequences combined with contrast-enhancing tumour parts and non-enhancing enclosed necrosis and cysts from T1w/T1c sequences. We used HD-BET for skull stripping and ANTsPY version 0.3.2 for image registration.
Normalization	Images were normalized/smoothed before registration to standard space and brain extraction was performed using HD-BET followed by a non-linear registration with cost-function masking to normalized space using ANTsPY. In ANTsPY we used the symmetric normalizations: affine+deformable transformation, with cross correlation as optimization metric ('SyN' option, with syn_metric set to 'CC' and affine shrink factors (8,4,2,1)).
Normalization template	Images were registered to MNI152 standard space at 2x2x2 mm spatial resolution.
Noise and artifact removal	Images were normalized/smoothed to remove artifacts by subtracting the lowest voxel value from the image.
Volume censoring	We used cost-function masking meaning that the tumour segmentation volume was excluded during registration and transformed according to the 'heatlhy' brain transformation matrix.

Statistical modeling & inference

Model type and settings	Multivariate methods were used. Two methods were considered; sparse canonical correlation analysis using the LESYMAP package and a Bayesian categorical multiple regression model run through Bambi with vaguely informative priors and four chains with 2000 draws.
Effect(s) tested	There was no task or stimulus as we used routine clinical MRI scans. We considered the Center for Epidemiologic Studies Depression scale (CES-D) as outcome measure/dependent variable and related this to the location of the brain tumor. For

Bayesian regression, patients were split into three groups according to CES-D; an absence of depressive symptoms, intermediate depressive symptoms and severe depressive symptoms.

Specify type of analysis: ☐ Whole brain ☐ ROI-based ☒ Both

Anatomical location(s) Anatomical locations were obtained by using probabilistic atlases of different brain structures.

Statistic type for inference

(See Eklund et al. 2016)

Sparse canonical correlation analysis is a clusterwise method. Voxels with identical lesion patterns are grouped together. At least three people had to have a lesion in a given voxel to be included. We used 1000 permutations, 10 folds and 10 cross validation repetitions. FDR corrected p-value was considered significant if $p<0.05$.
For the Bayesian model we calculated the overlap of tumor segmentation and parcel in different atlases and considered these measures as independent variables. Infiltrated parcels were considered significant if the posterior 94% highest density interval excluded zero.

Correction

False Discovery Rate for lesymap

Models & analysis

n/a	Involved in the study
☐	☒ Functional and/or effective connectivity
☐	☒ Graph analysis
☐	☒ Multivariate modeling or predictive analysis

Functional and/or effective connectivity

Processed connectivity matrices of 1000 human connectome project participants were used which included Pearson correlations to describe pairwise correlations or co-activations between brain regions.

Graph analysis

The CES-D scale was used as outcome measure/dependent value.
We averaged connectivity matrices to create a normative connectivity matrices and calculated graph measures local efficiency (LE) and eigenvector centrality (EC) for each parcel (node) with the correlations as weights.
For each patient we then removed completely infiltrated brain regions from the normative matrix and lowered the weight . We calculated LE and EC for the remaining parcels and subtracted these from the normative LE and EC values. To acquire a modeled functional network impact due to the tumour we calculated the median LE and EC difference of specific networks.

Multivariate modeling and predictive analysis

See previous section for all models used. The LE and EC difference per functional network were used as independent variables in Bayesian analysis.